SERS-active substrates based on embedded Ag nanoparticles in c-Si: modeling, technology, application

© A.A. Ermina[1], N.S. Solodovchenko[2], K.V. Prigoda[1,3], V.S. Levitskii[4], S.I. Pavlov[1], Yu.A. Zharova[1,¶]

[1] Ioffe Institute,
194021 St. Petersburg, Russia
[2] School of Physics and Engineering, ITMO University,
197101 St. Petersburg, Russia
[3] Peter the Great St. Petersburg Polytechnic University,
195221 St. Petersburg, Russia
[4] RnD Center TFTE,
194064 St. Petersburg, Russia
¶ E-mail: piliouguina@mail.ioffe.ru

Received May 5, 2023
Revised June 19, 2023
Accepted June 20, 2023

A simple method for obtaining $SiO_2:Ag:Si$ and $Ag:Si$ hybrid nanostructures is presented. High-temperature annealing of an Ag island film on the surface of c-Si makes it possible to preserve the plasmonic properties of Ag nanoparticles and protect them from external influences by coating them with a thermally grown layer of SiO_2. The calculation of the electric field strength distribution in the structure with embedded Ag nanoparticles in c-Si demonstrates the presence of intrinsic „hot spots“ at the corners of the nanoparticles, which leads to a maximum enhancement factor ($\sim 10^6$) of Raman scattering. A numerical calculation of the dependence of the spectral position of a localized plasmon resonance on the geometry of structures can serve as a basis for their design in the future. Surface-enhanced Raman scattering showed reliable detection of the methyl orange from an aqueous solution at a concentration of $< 10^{-5}$ M.

Keywords: SERS, Ag nanoparticles, c-Si, methyl orange, localized plasmon resonance.

DOI: 10.61011/SC.2023.04.56420.07k

1. Introduction

The current trend is to combine nano-plasmonics with well-developed semiconductor technology to create new functional hybrid structures for Raman scattering [1,2] signal amplification. Excitation of the localized plasmon resonance (LPR) in such structures by an external electromagnetic wave leads to the amplification of Raman scattering, namely Surface-enhanced Raman scattering (SERS), enhancement factor (EF) of which can reach 10^{11} [3]. The SERS is the method is one of the most sensitive non-destructive analytical methods with high response rates currently available. This method allows the detection and study of ultra-small amounts of a substance (analyte) down to single molecules, since the cross-section of Raman scattering of the analyte on the surface or near the metal increases by orders of magnitude [4]. SERS-active substrates based on silicon and noble metals provide significant electromagnetic enhancement of the Raman scattering associated with LPR excitation [5-7]. To achieve maximum enhancement factor, the position of the analyte absorption band maximum must be close to the spectral position of the LPR, which, in turn, depends on the structure morphology and the dielectric constant of the surrounding medium. For practical applications, the requirements for SERS-active substrates are: chemical inertness to analyte and external influences, stability and reproducibility. Therefore, investigating the influence of the geometry of SERS-active substrates on the LPR position will establish patterns that allow, by varying the structural parameters of the substrates, to control the sensitivity of the optical response in the visible and near-infrared spectral ranges. Due to all these qualities, the SERS method has attracted the attention of the scientific community; over the past four decades, the practical use of SERS-active substrates has increased dramatically in a wide variety of fields. For example, in medical diagnostics (studying viruses, cells, tissues, and DNA) [8–10]; in biochemistry and pharmaceuticals [11]; in forensics (identifying illegal and dangerous substances, authenticating products using spectral labelling technology) [12,13]; in ecology (detecting pollutants) [14,15]; in the food industry (testing for pesticides, etc.) [16,17].

In this paper, we propose structures with plasmonic properties based on silver nanoparticles (AgNPs) embedded in the volume of single-crystal silicon (c-Si) by high-temperature annealing to investigate the Raman amplification. In the annealing process, the simultaneous embeddence of AgNP into the volume of the c-Si substrate and covering them with a layer of thermally grown SiO_2. This layer protects the structure from external influences. Structures based on such a high-tech material as silicon are very promising for creating sensor chips [5]. Silver was chosen as the noble metal because theoretical [18] and experimental [19] studies of structures with silver nanoparticles and films have a higher extinction cross-section and thus a higher Raman signal enhancement compared to gold structures.

Thus, based on the investigated structures, it is possible to develop a reusable sensor as a SERS-active substrate.

2. Experiment

2.1. Fabrication of structures

c-Si *p*-types with a resistance of 10 Ohm · cm and a crystal-lattice orientation of (100) were used in this study. After standard RCA (Radio Corporation of America) cleaning of silicon wafers (Fig. 1, p. 1), an island film of Ag was formed on their surfaces by chemical deposition from a solution ($0.02\text{M}\ AgNO_3 + 5\text{M}\ HF$, in the ratio of 1 : 1) within 30 s (Fig. 1, p. 2). Further, the investigated structures were subjected to high-temperature annealing at 1000°C in an atmosphere of water vapor for 40 min (Fig. 1, p. 3). The SiO_2 layer was removed in dilute fluoric acid solution (20% HF) on several structures after annealing (Fig. 1, p. 4).

An aqueous solution of the organic dye methyl orange (MO) ($C_{14}H_{14}N_3NaO_3S$) with different concentrations was used as the analyte: 10^{-3}, 10^{-4} and 10^{-5} M. Droplets ($2\,\mu$l) were applied to each substrate, then air-dried. It should be noted that the Raman bands from MO are in the $832-1619\ \text{cm}^{-1}$ area and do not overlap with the characteristic peak for silicon in the $520\ \text{cm}^{-1}$ area. Therefore, it was MO that was chosen as an analyte over other known organic dyes [20].

Elemental and morphological analyzes of the hybrid structures were performed on a JSM-7001F scanning-electron microscope (SEM) (JEOL, Japan) in secondary electron mode and at an accelerating voltage of 5 kV,

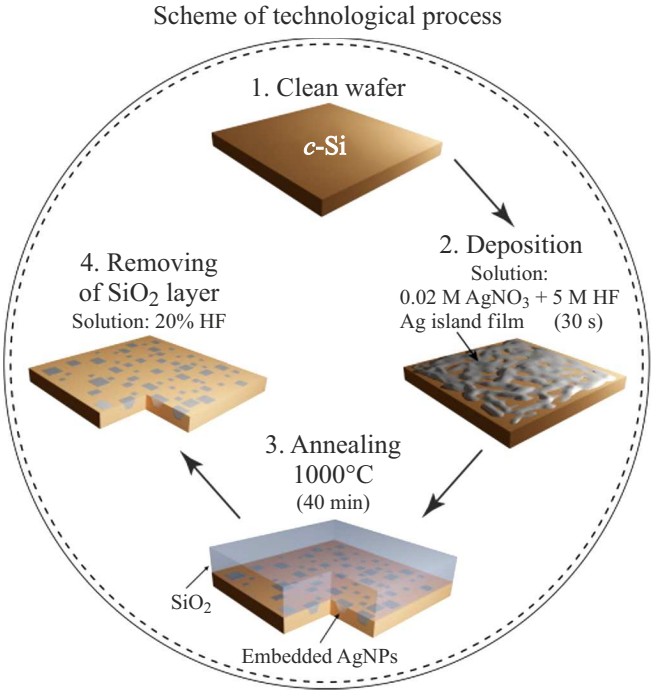

Figure 1. Schematic representation of the process steps for the manufacturing of SERS-active substrates.

Morphological parameters of structures after annealing for 40 min

Size l, nm	223 ± 106
Aspect ratio l/h	1.76 ± 0.34
Interparticle distance a, nm	297 ± 92
Coverage factor, %	39
Thickness of SiO_2, nm	510

equipped with an X-ray dispersive spectrometer. Statistical analysis of nanostructures before and after annealing was carried out using SEM images and ImageJ open-source image analysis and processing software, including the determination of the size of AgNP, the density of their coverage on the silicon wafer surface (coverage factor), and the interparticle distance. After annealing, silicon dioxide thicknesses and transverse dimensions of AgNP were measured on the cross section of the SEM structures. The cross-sectional microanalysis of the obtained structures in the reflected electron mode was carried out by energy-dispersive X-ray spectroscopy.

IR transmittance spectra were measured on an IRPrestige-21 IR Fourier spectrophotometer with an AIM-8000 IR microscope (Shimadzu Corp., Japan). Measurable spectral range $1.4-11\,\mu$m.

The Raman scattering and SERS spectra were measured on a Labram HR800 spectrometer (HORIBA, France) equipped with a laser generating radiation at a wavelength of 532 nm with a power of $60\,\mu$W to prevent analyte damage. A 600 strokes/mm lattice was used during the measurements, and an Olympus $100\times$ lens (NA = 0.9) was used to focus the laser beam on the sample surface into a spot with a diameter of $\sim 1\,\mu$m.

2.2. Calculation method

The optical properties of the structures was numerically modelled with the commercial software COMSOL Multiphysics using the finite element method (FEM). To describe the basic optical dependences, it is sufficient to use a 2D model, which is an approximation to real structures, which allowed not to resort to long and high-cost calculations [21]. A schematic 2D model of the structure with embedded AgNP in *c*-Si is shown in Fig. 2. Along the axis x, periodic boundary conditions were used. Light is incident along the axis y at the normal angle of incidence. A perfectly matched layer (PML) was used on the top and bottom of the model to ignore wave reflection from the boundaries. The geometric parameters of the 2D model of the structure were obtained from analyzing SEM images of the structures (see table).

3. Results and discussion

3.1. Calculations

The influence of the geometrical parameters of the structures (period (a), size (l), height (h) of the AgNP,

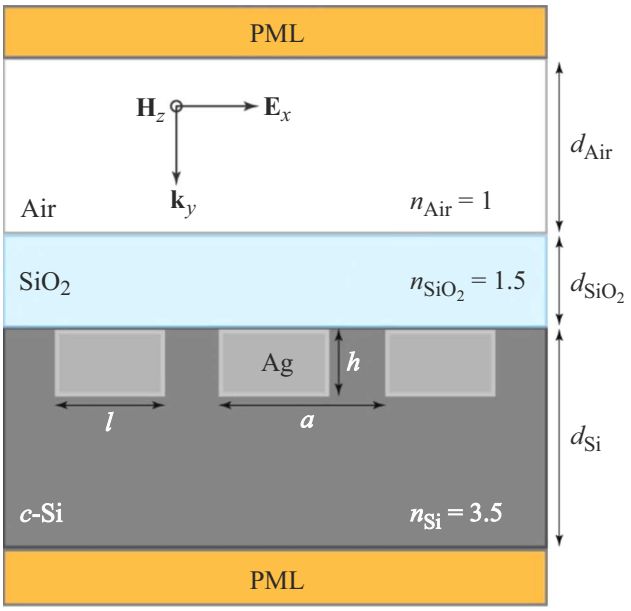

Figure 2. Schematic 2D model used in the calculations for the embedded AgNP under annealing for 40 min, where a is lattice period, l is AgNP length, h is AgNP height, d is thicknesses and n is refraction index of the layers.

and the thickness of the layer SiO_2 (d_{SiO_2})) on the position of the low-frequency (dipole mode) LPR was investigated during the numerical simulation. At the first stage it was necessary to determine at what ratio of the interparticle distance (period) to the nanoparticle size the LPR position will change insignificantly, i. e. there will be a weak interaction between nanoparticles. This is necessary to exclude complex interactions between particles from the calculations and investigate only the effect of nanostructure geometry on the LPR position. Fig. 3, *a* shows the dependences of the LPR position on the aspect ratio of period to size of nanoparticles without SiO_2 ($d_{SiO_2} = 0$) coating layer, determined from the absorption coefficient maximum in the spectra.

The calculations shown in Fig. 3 are done for the sizes (l) of 100, 150, 200 and 250 nm nanoparticles. The vertical dashed line in Fig. 3, *a* ($a/l = 1.5$) separates the areas where the position of the LPR strongly depends on the aspect ratio (coupling area) and where the change of the LPR position is insignificant (weak coupling area). For further calculations of the LPR position as a function of the aspect ratio, the value of $a/l = 1.5$, at which there is a weak contribution from the interparticle interaction was fixed. The insert shows the distribution of the electric field strength $|\mathbf{E}|$ between two AgNP with $l = 100$ nm for the aspect ratio a/l, represented by the black dot in the interaction area between the particles.

Fig. 3, *b* shows the dependences of the LPR position on the aspect ratio of the nanoparticle size to its height (l/h). The blue area corresponds to a standard deviation (σ_1) on the aspect ratio (l/h) equal to 0.34 (see table). In calculations for nanoparticle sizes > 200 nm, a diffraction mode is observed that distorts the low-frequency LPR mode, which is well demonstrated by the behavior of the curve for $l = 250$ nm at the aspect ratio $l/h > 1.76$. The insert to Fig. 3, *b* shows the electric field strength distribution $|\mathbf{E}|$ between the interaction AgNP with an aspect ratio of 1.76 indicated in the black dot.

The dependence of the LPR position on the thickness of the SiO_2-layer coating was also calculated. The calculation showed weakly pronounced sinusoidal deviations of the LPR position from the LPR position without SiO_2.

Using the dependences presented in Fig. 3, it is possible to design structures of given sizes, to expect the manifes-

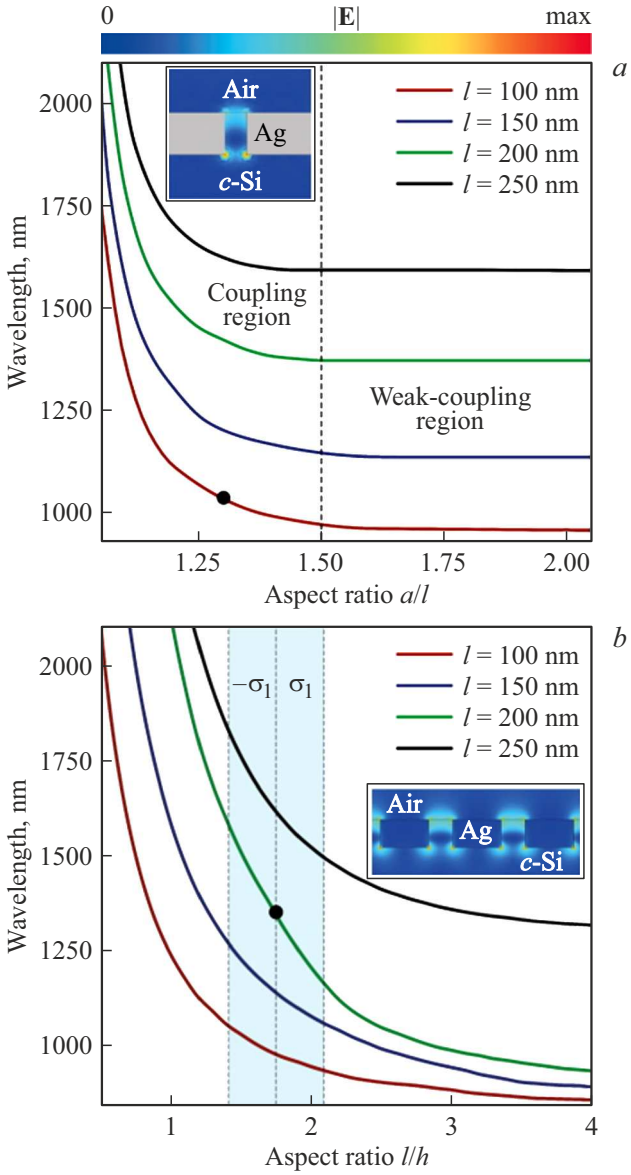

Figure 3. *a* is dependencies of the LPR position on the aspect ratio a to l (100, 150, 200, 250 nm) AgNP; *b* is dependencies of the LPR position on the aspect ratio l (100, 150, 200, 250 nm) to h AgNP. (A color version of the figure is provided in the online version of the paper).

tation of low-frequency LPR and, as a consequence, the enhancement of Raman signal in certain wavelength ranges. Such a prediction is important for the development of SERS-active substrates.

In order to qualitatively study the optical properties of embedded AgNP in c-Si substrate, we have developed a 3D model ($d_{SiO_2} = 0$) in COMSOL Multiphysics with periodic boundary conditions. An intermediate size of the embedded nanoparticle $l = 150$ nm with aspect ratios of $a/l = 1.5$ and $l/h = 1.76$ was chosen. The enhancement factor ($EF_{Ag/Si}$) of the presented system was estimated as [22,23]

$$EF_{Ag/Si} = \frac{1}{S} \iint_S \frac{|\mathbf{E}_{Ag/Si}|^4}{|\mathbf{E}_0|^4} dS, \qquad (1)$$

where $\mathbf{E}_{Ag/Si}$ and $\mathbf{E}_0$ — local and incident electric field strength vectors, respectively; S — integration surface located at a distance of 0.1 nm from the air — Ag/Si boundary.

Thus, the maximum enhancement factor from the structure was $EF_{Ag/Si} = 1.1 \cdot 10^6$ at a wavelength of 795 nm. The presence of right angles in a metallic nanoparticle leads to a strong localization of the field at these angles, namely to the formation of intrinsic „hot spots“. In the result, the scattered field from MO molecules attached to the surface of the SERS-active substrate strongly increases. At a wavelength of 532 nm, which corresponds to the emission of the laser in the experiment, $EF_{Ag/Si} = 1.4 \cdot 10^3$. For comparison, EF from a silicon substrate without embedded AgNP was calculated to be $EF_{Si} = 0.03$. For the structure with a thick layer SiO_2 (~ 500 nm) $EF_{SiO_2/Ag/Si} \sim 10$.

3.2. Morphological characterization of structures

Fig. 4 shows SEM images of the structures after annealing the Ag island film on 1000°C for 40 min.

The table shows the values of size (l), aspect ratios of size to height (l/h), interparticle spacing (a), AgNP surface fill factor c-Si, and layer thickness SiO_2.

Fig. 4, c shows that during annealing for 40 min, the AgNP are completely embedded in the volume of the silicon wafer and covered by the SiO_2 layer. It should be noted that AgNP, embedding into the silicon wafer, acquire the shape of an inverted pyramid (Fig. 4, b). This is due to the local variation of SiO_2 growth rates under AgNP and the manifestation of oxidation anisotropy during high-temperature annealing of silicon. The pyramid faces are planes (111) with the lowest oxidation rate, and AgNP completely fills the resulting voids.

3.3. Optical properties of structures

The results of studies using the spectrascopic ellipsometry method of AgNP on the c-Si surface after chemical deposition are discussed in detail by us in [24,25]. Ag island films with layer thickness ~ 50 nm exhibit a resonance

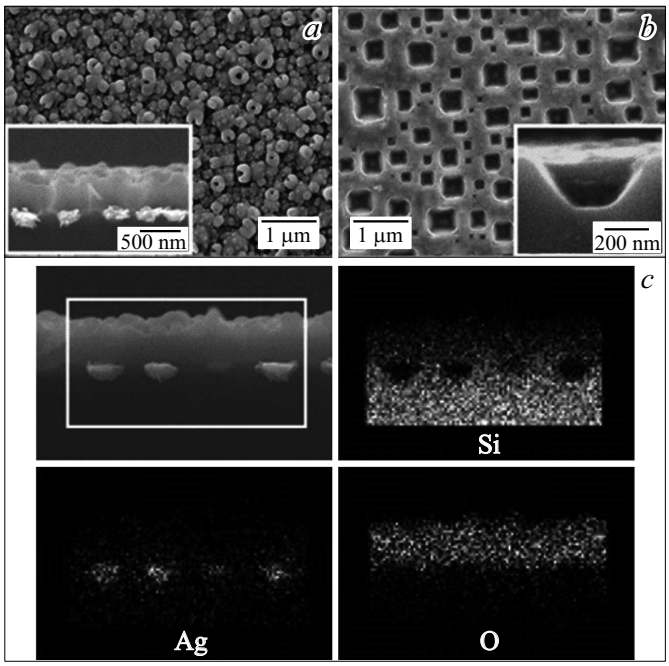

Figure 4. SEM images of the structure after annealing: a is top view (insert — cross-section); b is top view after AgNP removal (insert — cross-section); c is cross-section of the structure, with the frame highlighting the area where the energy-dispersive X-ray analysis of elements was performed.

feature in the permittivity spectra — plasmon resonance in the longitudinal mode ($E = 3.9$ eV), with the complex permittivity ε close to bulk Ag.

Investigations of the transmittance spectra of the obtained structures are presented in Fig. 5. Silicon has good transparency in the range of 1.2 μm or more, in contrast to the visible spectral range, where transmittance spectra cannot be measured. In the range from 1.6 to 2.5 μm, a minimum transmittance ($< 7\%$) is observed for the samples after high-temperature annealing, compared to the c-Si spectrum, and its value approaches the value of Ag island films. This is probably due to the partial absorption of radiation on AgNP. The band $\sim 9.1\,\mu$m in Fig. 5 is characterized by oxygen absorption. This dip in transmittance is due to the thick SiO_2 (~ 510 nm) layer on the structure.

To avoid possible overlap of the analyte's Raman bands with the characteristic Raman bands of the fabricated samples, the measurements shown in Fig. 6 were carried out. Raman scattering spectra of initial wafers: pure silicon substrate, Ag island film, and structures after annealing for 40 min. All spectra show a line in the area 520 cm^{-1}, corresponding to scattering on optical phonons of the 1st order of the crystal lattice c-Si and a less intense Raman band of the 2nd order for Si (940–980 cm^{-1}) [26]. Also, the spectrum from the sample with Ag island film (green line) clearly shows an intense band at ~ 240 cm^{-1} due to the valence vibrations of bonds Ag–N [27].

It is important to note that the structures obtained after annealing do not show any bands other than the characteristic lines for *c*-Si. In this case, for the Ag island film, the 520 cm^{-1} band is strongly suppressed and the band (940–980 cm^{-1}) is almost completely absent. For the structures after annealing, a slight decrease in the intensity of the characteristic bands for *c*-Si at 520 and 940–980 cm^{-1} was observed.

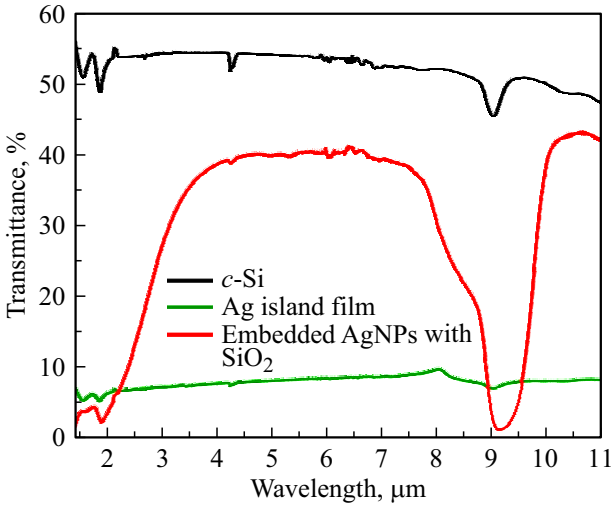

Figure 5. Transmittance spectra of the investigated structures: black line is *c*-Si; green line is Ag island film; red line is embedded AgNP coated with a layer of SiO_2.

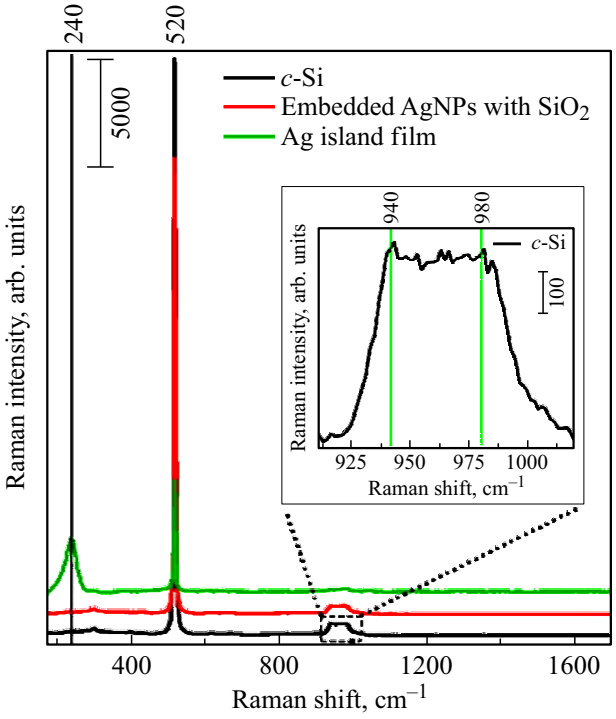

Figure 6. Raman scattering spectra of samples without MO: black line is Raman spectrum of pure *c*-Si wafers; red line is Raman spectrum of the structure with embedded AgNP coated with layer SiO_2; green line is Raman spectrum of island film Ag.

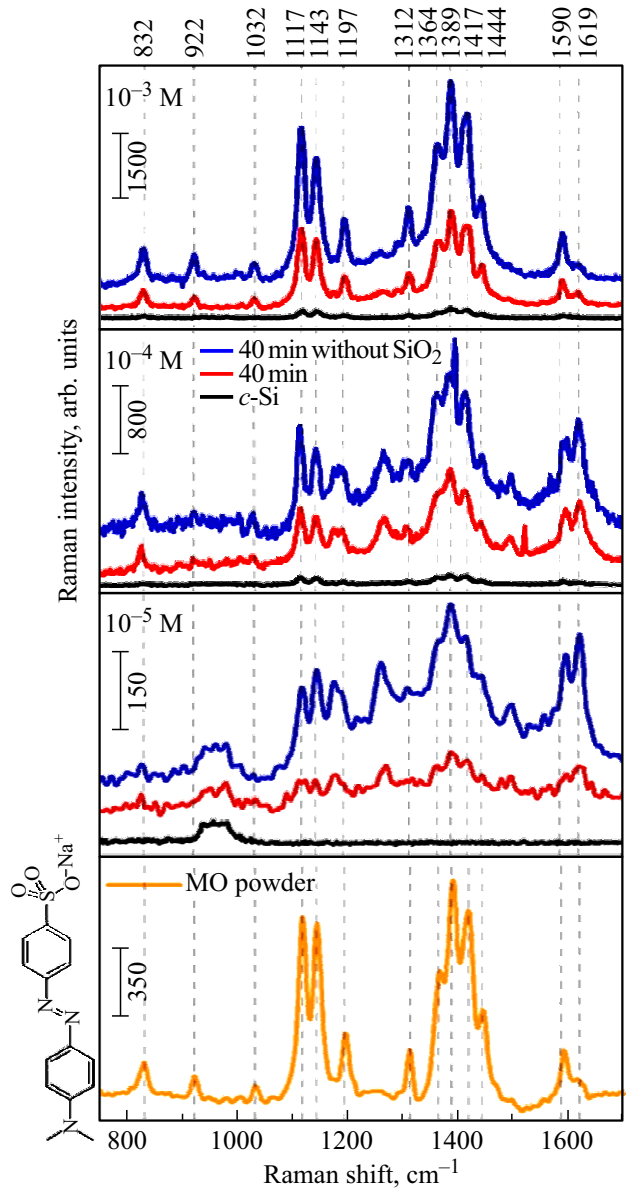

Figure 7. SERS spectra of MO at different concentrations of 10^{-3}, 10^{-4} and 10^{-5} M and the Raman spectrum of MO powder on quartz substrate. Black line is original *c*-Si substrate, red line is embedded AgNP under the SiO_2 layer, blue line is embedded AgNP with the SiO_2 layer removed.

Fig. 7 shows the spectrum of the initial MO material in powder form (orange line), where all characteristic peaks of MO are clearly visible. Raman peaks of MO powder: 832, 922, 1032, 1117, 1143, 1197, 1312, 1364, 1389, 1417, 1444, 1590, 1619 cm^{-1} (Fig. 7), which clearly coincides with the data [28]. The band at 922 cm^{-1} $\nu(C-N)_{Me}$ indicates a methyl group, and 1032 cm^{-1} refers to aromatic rings [28]. According to the source [29], the peaks at 1197 cm^{-1}/1117 cm^{-1} show $\nu(Ph-N)+\delta(C-H)$ valence and strain vibrations (where Ph — phenyl group). Bands at 1143 cm^{-1} — due to $\delta(C-H)$ strain fluctuation. At 1364 cm^{-1} there are $\nu(C-N)_{Me}+\delta(C-C)+\delta(C-H)$

valence and strain vibrations. At $1417\,cm^{-1}/1389\,cm^{-1}$ shows $\nu(N{=}N) + \nu(C{-}C) + \delta(C{-}H)$ valence and strain vibrations. At $1444\,cm^{-1}$ $\nu(C{-}C)$ is valence fluctuation. At $1590\,cm^{-1}/1619\,cm^{-1}$ are due to $\nu(C{-}C) + \delta(C{-}C)$ valence and strain fluctuations. The absorption of the MO molecule on the surface with Ag is via the N=N group, so the most intense bands are observed at $1417\,cm^{-1}/1389\,cm^{-1}$ because of the very strong valence vibration $\nu(N{=}N)$ [29].

Next, an aqueous solution of organic MO dye was applied to the structures investigated in this work, the details of the application are described in Section 2.1. SERS spectra was measured as a function of analyte concentration (blue, red, and black lines in Fig. 7). Measurements were taken at different points across the samples to reproduce the measurements and to verify the uniformity of the properties of the structures across the area. Fig. 7 shows the averaged spectra, the deviation from the mean is $< 10\%$, which confirms the high reproducibility of the results, despite the disordered structure and size variation of AgNP. For comparative analysis, aqueous solutions of MOs were also deposited on the clean c-Si substrate (black line in Fig. 7). On clean c-Si substrates, it is not possible to detect a clear signal from the MO for all investigated concentrations because there is no local electromagnetic field enhancement. Although the main MO bands are clearly visible for the MO concentration $10^{-5}\,M$ (Fig. 7) on the structures with AgNP, a broad band at $940{-}980\,cm^{-1}$ characteristic of c-Si is also observed. When the concentration of MO increases from 10^{-4} to $10^{-3}\,M$, we see a complete disappearance of the c-Si bands and an enhancement of the Raman scattering MO signal. It should be noted that at the thickness of the layer $SiO_2 \sim 510\,nm$, covering AgNP, the intensity of the Raman scattering signal sharply decreases, which is associated with a decrease in sensitivity, since there is no contact of the analyte with its own „hot spots“, most of the MO peaks become less pronounced and strongly blurred. At the same time, the most intense MO bands associated with the strong valence vibrations of $\nu(N{=}N)$ at $1417\,cm^{-1}/1389\,cm^{-1}$ are clearly visible. The bands at $1197\,cm^{-1}/1312\,cm^{-1}$ for concentrations 10^{-4} and $10^{-5}\,M$ are blurred and shifted, possibly due to the chemical bond lengths of the analyte. Shorter MO bond lengths cause a shift towards higher wave numbers and vice versa. Accordingly, if the length of the MO chemical bond changes, there will be a shift in the Raman scattering [28].

The experimental value of $EF_{Ag/Si}$ was $EF_{exp} = 2.5 \cdot 10^3$, the order of which is the same as the numerically calculated EF presented in Section 3.1. The ratio of values of the same peak, e.g. at $1389\,cm^{-1}$ (Fig. 7) for the structure with embedded AgNP with MO and c-Si substrate with MO of the same concentration was examined.

4. Conclusion

In result of this paper, SERS-active substrates based on single crystal silicon and silver nanoparticles were prepared. The hybrid structures were formed by high-temperature annealing (1000°C) of the initial structure — island Ag film formed by chemical deposition. Thus, structures with embedded Ag particles in c-Si were obtained with an average size of $223 \pm 106\,nm$. The thickness of the thermally grown SiO_2 layer, which protects the AgNP from external influence, was $\sim 510\,nm$.

Numerical calculations have shown that such structures possess the presence of LPR in a wide (near-IR) spectral range depending on the size of AgNP and their interparticle distance. At the same time, because of the strong localization of the electromagnetic field exactly on the metal nanoparticle, structures with a large SiO_2 layer may be less effective as SERS-active substrates because of a sharp drop in sensitivity. Also, the calculations showed that the structures with a given period of embedded AgNP without SiO_2 protective layer exhibit the maximum SERS enhancement factor $\sim 10^6$.

SERS studies of MO demonstrate high analyte detection on fabricated structures without SiO_2. The presence of blurred peaks and intensity reduction for structures with the presence of SiO_2 could possibly be resolved by optimizing the thickness of SiO_2, the size of the AgNP and the interparticle distances. From numerical calculations and experimental data, it is clearly seen that a promising development of such structures is the creation of ordered structures, which will sharply increase the presence of intrinsic „hot spots“ at the corners of nanoparticles and, as a consequence, will lead to a sharp increase in the SERS enhancement factor. By combining semiconductor technology and nanoplasmonics, it will be possible to create chips for use as SERS-active substrates in a single process cycle.

Acknowledgments

The authors are grateful to A.A. Krasilin for discussion of the article materials.

Funding

The paper was supported by the Ministry of Science and Higher Education of the Russian Federation within the framework of the state order No. 0040-2019-0012).

Conflict of interest

The authors declare that they have no conflict of interest.

References

[1] J. Langer, et. al. ACS Nano, **14**9 (1), 28 (2020). https://doi.org/10.1021/acsnano.9b04224
[2] R. Wu, T. Mathieu, C.J. Storey, Q. Jin, J. Collins, L.T. Canham, A. Kaplan. Adv. Optical Mater., **9**, 2002119 (2021). https://doi.org/10.1002/adom.202002119
[3] C. Zong, M. Xu, L.-J. Xu, T. Wei, X. Ma, X.-S. Zheng, R. Hu, B. Ren. Chem. Rev., **118** (10), 4946 (2018). https://doi.org/10.1021/acs.chemrev.7b00668

[4] L. Xie, H. Zeng, J. Zhu, Z. Zhang, W. Xia. Nano Res., **15**, 4374 (2022). https://doi.org/10.1007/s12274-021-4017-4
[5] Q. Zou, S. Mo, X. Pei, Y. Wang, T. Xue, M. Mayilamu, G. Qin. AIP Advances, **8**, 085302 (2018). https://doi.org/10.1063/1.5039600
[6] J. Wang, Z. Jia, C. Lv. Opt. Express, **26**, 6507 (2018). https://doi.org/10.1364/OE.26.006507
[7] A.A. Ermina, N.S. Solodovchenko, K.V. Prigoda, V.S. Levitskii, V.O. Bolshakov, M.Yu. Maximov, Yu.M. Koshtyal, S.I. Pavlov, V.A. Tolmachev, Yu.A. Zharova. Appl. Surf. Sci., **608**, 155146 (2023). https://doi.org/10.1016/j.apsusc.2022.155146
[8] Z. Zhang, J. Wang, K.B. Shanmugasundaram, B. Yeo, A. Möller, A. Wuethrich, L.L. Lin, M. Trau. Small, **16**, 1905614 (2020). https://doi.org/10.1002/smll.201905614
[9] S. Bamrungsap, A. Treetong, C. Apiwat, T. Wuttikhun, T. Dharakul. Microchim. Acta, **183**, 249 (2016). https://doi.org/10.1007/s00604-015-1639-9
[10] W. Kim, S.H. Lee, J.H. Kim, Y.J. Ahn, Y.-H. Kim, J.S. Yu, S. Choi. ACS Nano, **12** (7), 7100 (2018). https://doi.org/10.1021/acsnano.8b02917
[11] D. Zhang, P. Liang, Z. Yu, J. Xia, D. Ni, D. Wang, Y. Zhou, Y. Cao, J. Chen, J. Chen, S. Jin. J. Hazard. Mater., **382**, 121023 (2020). https://doi.org/10.1016/j.jhazmat.2019.121023
[12] W. Fan, S. Yang, Y. Zhang, B. Huang, Z. Gong, D. Wang, M. Fan. ACS Sensors, **5** (11), 3599 (2020). https://doi.org/10.1021/acssensors.0c01908
[13] T. Liyanage, A. Rael, S. Shaffer, S. Zaidi, J.V. Goodpaster, R. Sardar. Analyst, **143**, 2012 (2018). https://doi.org/10.1039/C8AN00008E
[14] H. Sun, X. Li, Z. Hu, C. Gu, D. Chen, J. Wang, B. Li, T. Jiang, X. Zhou. Appl. Surf. Sci., **556**, 149748 (2021). https://doi.org/10.1016/j.apsusc.2021.149748
[15] X. He, X. Zhou, Y. Liu, X. Wang. Sensors Actuators B: Chem., **311**, 127676 (2020). https://doi.org/10.1016/j.snb.2020.127676
[16] Z. Deng, X. Chen, Y. Wang, E. Fang, Z. Zhang, X. Chen. Anal. Chem., **87** (1), 633 (2015). https://doi.org/10.1021/ac503341g
[17] J. Chen, Y. Huang, P. Kannan, L. Zhang, Z. Lin,J. Zhang, T. Chen, L. Guo. Anal. Chem., **88** (4), 2149 (2016). https://doi.org/10.1021/acs.analchem.5b03735
[18] E. Galopin, J. Niedziołka-Jönsson, A. Akjouj, Y. Pennec, B. Djafari-Rouhani, A. Noual, R. Boukherroub, S. Szunerits. J. Phys. Chem. C, **114** (27), 11769 (2010). https://doi.org/10.1021/jp1023839
[19] K. Kneipp, M. Moskovits, H. Kneipp. *Surface-Enhanced Raman Scattering: Physics and Applications* (Springer Verlag Berlin–Heidelberg, 2006). https://doi.org/10.1007/3-540-33567-6
[20] M.-C. Wu, M.-P. Lin, S.-W. Chen, P.-H. Lee, J.-H. Li, W.-F. Su. RSC Advances, **4**, 10043 (2014). https://doi.org/10.1039/C3RA45255G
[21] E. Galopin, A. Noual, J. Niedziołka-Jönsson, A. Akjouj, Y. Pennec, B. Djafari-Rouhani, A. Noual, R. Boukherroub, S. Szunerits. J. Phys. Chem. C, **113**, 15921 (2009). https://doi.org/10.1021/jp905154z
[22] R.P. Van Duyne (ed. by C.B. Moore). (N.Y., Academic Press, 1979) p. 101.
[23] P. Hildebrandt, M. Stockburger. J. Phys. Chem., **88**, 5935 (1984). https://doi.org/10.1021/j150668a038
[24] V.A. Tolmachev, E.V. Gushchina, I.A. Nyapshaev, Yu.A. Zharova. Thin Sol. Films, 139352 (2022). https://doi.org/10.1016/j.tsf.2022.139352
[25] Y. Zharova, A. Ermina, S. Pavlov, Y. Koshtyal, V. Tolmachev. Phys. Status Solidi A, **216**, 1900318 (2019). https://doi.org/10.1002/pssa.201900318
[26] U. Kreibig, M. Vollmer. *Optical Properties of Metal Clusters* (Springer Series in Materials Science, 1995). doi:10.1007/978-3-662-09109-8
[27] J. Chowdhury, M. Ghosh. J. Colloid Interface Sci., **277**, 121 (2004). https://doi.org/10.1016/j.jcis.2004.04.030
[28] A. Zarei, A. Shafiekhani. Mater. Chem. Phys., **242**, 122559 (2020). https://doi.org/10.1016/j.matchemphys.2019.122559
[29] M.Z. Si, Y.P. Kang, Z.G. Zhang. Appl. Surf. Sci., **255** (11), 6007 (2009). https://doi.org/10.1016/j.apsusc.2009.01.055

Translated by Y.Deineka